Fully Conjugated Three-Dimensional Thiazole-Based Covalent Organic Framework Exhibiting Hierarchical Microtubular Architecture

Ignacio Munoz-Alonso,[a,b] Johannes Sigl,[b] Markus Döblinger,[a] Tianhao Xue,[a] Ivan Huc[b*] and Thomas Bein[a*]

[a]Department of Chemistry and Center for Nanoscience(CeNS), Ludwig-Maximilians-Universität Munich, Butenandstrasse 5-13, 81377 Munich, Germany.

*Email: bein@lmu.de

[b]Department of Pharmacy, Ludwig-Maximilians-Universität Munich, Butenandstrasse 5-13, 81377 Munich, Germany.

*Email: ivan.huc@cup.lmu.de

1. Methods:

Nuclear magnetic resonance (NMR) spectra were recorded on the spectrometers Avance III HD 400 MHz Bruker BioSpin and Avance III HD 500 MHz Bruker Biospin at 400 MHz and 500 MHz (proton spectra). Proton chemical shifts are expressed in parts per million (δ-scale) and are calibrated using residual non-deuterated solvent peaks as internal reference (^{1}H NMR: $CDCl_3$: 7.26, ^{13}C NMR: $CDCl_3$: 77.0).

UV-Vis spectra were recorded using a Perkin-Elmer Lambda 1050 spectrometer equipped with a 150 mm integrating sphere. Diffuse reflectance spectra were recorded using a Harrick Praying Mantis accessory kit and were referenced to barium sulfate as the white standard.

LC-MS chromatograms under acidic conditions were recorded on a Thermo Scientific Dionex UltiMate 3000 equipped with a C18 gravity (2.1 x 50 mm) with a flow of 0.33 mL min^{-1}. A concentration of 0.1% formic acid in water (A) and 0.1% formic acid in acetonitrile (B) were used as mobile phase. The LC system was coupled to a micrOTOF II mass spectrometer by Bruker Daltonics and molecules were ionized by ESI.

Nitrogen sorption isotherms were recorded on a Quantachrome Autosorb 1 at 77 K within a pressure range of p/p_0 = 0.001 to 0.98. Prior to the measurement of the sorption isotherms, the samples were heated for 24 h at 120 °C under turbo-pumped vacuum. For the evaluation of the surface area, the BET model was applied between 0.0005 and 0.08 p/p_0. Pore size distributions were calculated using the NLDFT adsorption model for cylindrical pores.

Single crystal X-ray diffraction (SCXRD) was measured on a Rigaku XtaLAB Synergy R, HyPix-Arc 150 with Cu K_α radiation from a PhotonJet Rotating-anode X-ray Source at 100 K. Data processing was performed in CrysAlisPro (V. 1.171.43.130a).[1] The structures were solved by direct methods and preliminarily refined in the AutoChem-6 [2] pipeline in CrysAlisPro. Further refinements were carried out with the SHELXL package through Olex2 1.5-ac6-020.[3,4] All non-hydrogen atoms were refined anisotropically. Hydrogen atom positions were calculated geometrically and refined using the riding model. Crystallographic data were deposited in the CCDC and are available under the accession number 2513710.

Powder X-ray diffraction (PXRD) measurements were performed using a Bruker D8 Discover diffractometer with Ni-filtered Cu K_α radiation and a LynxEye position-sensitive detector.

The initial structure model of the COF was built using the Forcite module of the Accelrys Materials Studio software package. For the COTz-1P COF, we applied a tetragonal crystal system with the highest possible symmetry in the space group $I4_1$. Experimental PXRD data were used for the respective Rietveld and Pawley refinements to optimize the structure models.

Transmission electron microscopy (TEM) was performed on a probe-corrected FEI Titan Themis instrument equipped with a field emission gun operated at 300 kV.

Scanning electron microscopy (SEM) images were recorded with an FEI Helios NanoLab G3 UC scanning electron microscope equipped with a field emission gun operated at 3 – 5 kV.

Photoluminescence (PL) data were processed with a FluoTime 300 instrument from PicoQuant GmbH. The samples were photo-excited using a laser with suitable wavelength according to the sample absorption, in this case 378 nm (LDH-P-C-375 from PicoQuant GmbH) pulsed at 40 MHz, with a pulse duration of ~100 ps and fluence of ~ 300 nJ cm^{-2}/pulse. The PL was collected using a high-resolution monochromator and photomultiplier detector assembly (PMA-C 192-N-M, PicoQuant GmbH).

2. Linker synthesis:

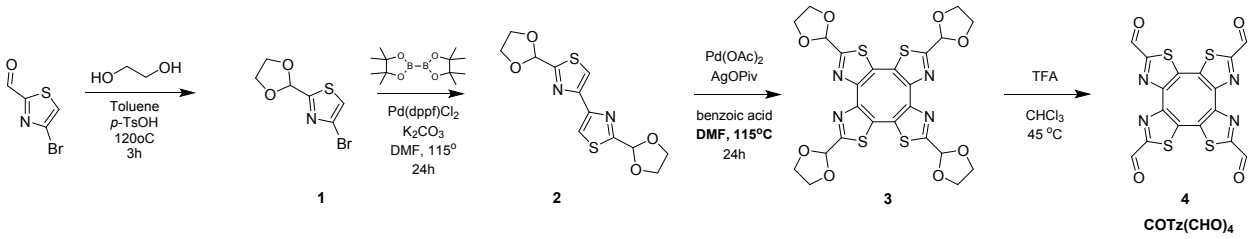

Synthesis of 4-bromo-2-(1,3-dioxolan-2-yl)thiazole (1):

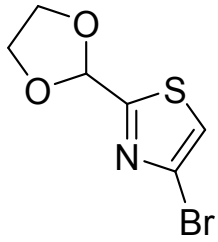

Into a 250 mL two-necked Schlenk-flask, under inert conditions, a solution of 4-bromo-2-formylthiazole (5 g, 26.03 mmol, 1.0 eq) in 50 mL toluene was added ethylene glycol (3.64 mL, 65.09 mmol, 2.5 eq) and *p*-toluenesulfonic acid monohydrate (247.6 mg, 1.3 mmol, 5 mol%). The reaction was refluxed at 120 °C overnight. After cooling to room temperature, water (100 mL) was added and the solution was extracted with ethyl acetate and washed with brine solution three times. The combined organic phases were dried over $MgSO_4$ and concentrated under reduced pressure. Purification via column chromatography (silica gel, DCM) yielded the title compound as a yellow oil (5.50 g, 23.43 mmol, 90 %).

^{1}H NMR (500 MHz, CDCl3): 7.27 (s, 1H), 6.12 (s, 1H), 4.14 (m, 2H), 4.08 (m, 2H).

Synthesis of 2,2'-di(1,3-dioxolan-2-yl)-4,4'-bithiazole (2)

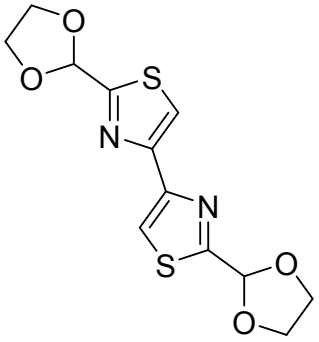

Into a 250 mL two-necked Schlenk-flask under inert conditions were added compound **1** (2.2 g, 9.36 mmol, 1.0 eq), bis(pinacolato)diboron (1.43 g, 5.62 mmol, 0.6 eq), $Pd(dppf)Cl_2$ (370 mg, 0.5

mmol, 0.05 eq), and K_2CO_3 (5.2 g, 37.44 mmol, 4.0 eq). The flask was degassed and re-filled with N_2 three times, and then 50 mL of DMF was added. The reaction was conducted at 115 ^oC overnight. After cooling to room temperature, water (100 mL) was added and the solution was extracted with DCM and washed with brine solution three times. The combined organic phases were dried over $MgSO_4$ and concentrated under reduced pressure. Purification via column chromatography (silica gel, DCM) yielded compound **2** as a bright white powder (950 mg, 3.04 mmol, 65 %).

^1H NMR (500 MHz, $CDCl_3$): 7.86 (s, 2H), 6.18 (s, 2H), 4.19 (m, 4H), 4.10 (m, 4H).

^{13}C NMR (500 MHz, $CDCl_3$): 168.71, 151.27, 116.60, 100.30, 65.78.

Synthesis of 2,5,8,11-tetra(1,3-dioxolan-2-yl)cycloocta[1,2-*d*:4,3-*d'*:5,6-*d''*:8,7 *d'''*] tetrakis(thiazole) (3)

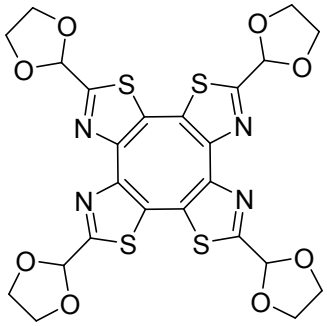

Into a 100 mL three-necked flask under inert conditions were added compound **2** (950 mg, 3.04 mmol, 1.0 eq), $Pd(OAc)_2$ (134 mg, 0.6 mmol, 0.2 eq) and AgOPiv (1.5 g, 9.12 mmol, 3.0 eq). The flask was degassed and filled with N_2 three times, and then 25 mL of DMF was added. The reaction was conducted at 115 ^oC during 72 h. After cooling to room temperature, $NaHCO_3$ was added and extracted with DCM. The combined organic phases were dried over $MgSO_4$ and concentrated under reduced pressure. Purification via column chromatography (silica gel, DCM:EtOAc = 99:5) yielded compound **3** as a pale-white powder (300 mg, 0.68 mmol, 45 %).

^1H NMR (500 MHz, $CDCl_3$): 6.15 (s, 4H), 4.19 - 4.07(m, 16H).

^{13}C NMR (500 MHz, $CDCl_3$): 171.58, 148.04, 127.85, 100.18, 66.09, 65.60.

HRMS: (ESI^+) m/z calc. for $C_{24}H_{21}O_8N_4S_4$: 621.0237 [M+H]+; found: 621.0376

Cycloocta[1,2-d:4,3-d':5,6-d'':8,7-d''']tetrakis(thiazole)-2,5,8,11-tetracarbaldehyde ($COTz(CHO)_4$) (4)

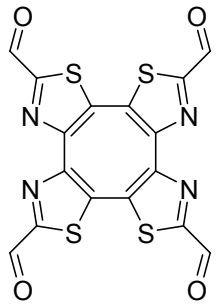

Into a 250 mL round bottom flask compound **3** (300 mg, 0.68 mmol,1.0 eq) was dissolved in 25 mL $CHCl_3$. After adding 1 mL H_2O and 10 mL trifluoroacetic acid (TFA), the reaction mixture was stirred at 40 ^oC overnight. The reaction mixture was then slowly added to 300 mL saturated aqueous $NaHCO_3$ solution and extracted with DCM. The organic phase was thoroughly washed with H_2O, dried over $MgSO_4$ and concentrated under reduced pressure. Purification by column chromatography (silica gel, DCM + 10% EtOAc) yielded the title compound as a yellow powder (286 mg, 0.65 mmol, 95%).

^1H NMR (500 MHz, $CDCl_3$): 10.04 (s, 4H)

^{13}C NMR (500 MHz, $CDCl_3$): 183.08, 168.70, 149.05, 132.72

HRMS: (ESI^+) m/z calc. for $C_{16}H_5O_4N_4S_4$: 444.9188 $[M+H]^+$; found: 444.9191.

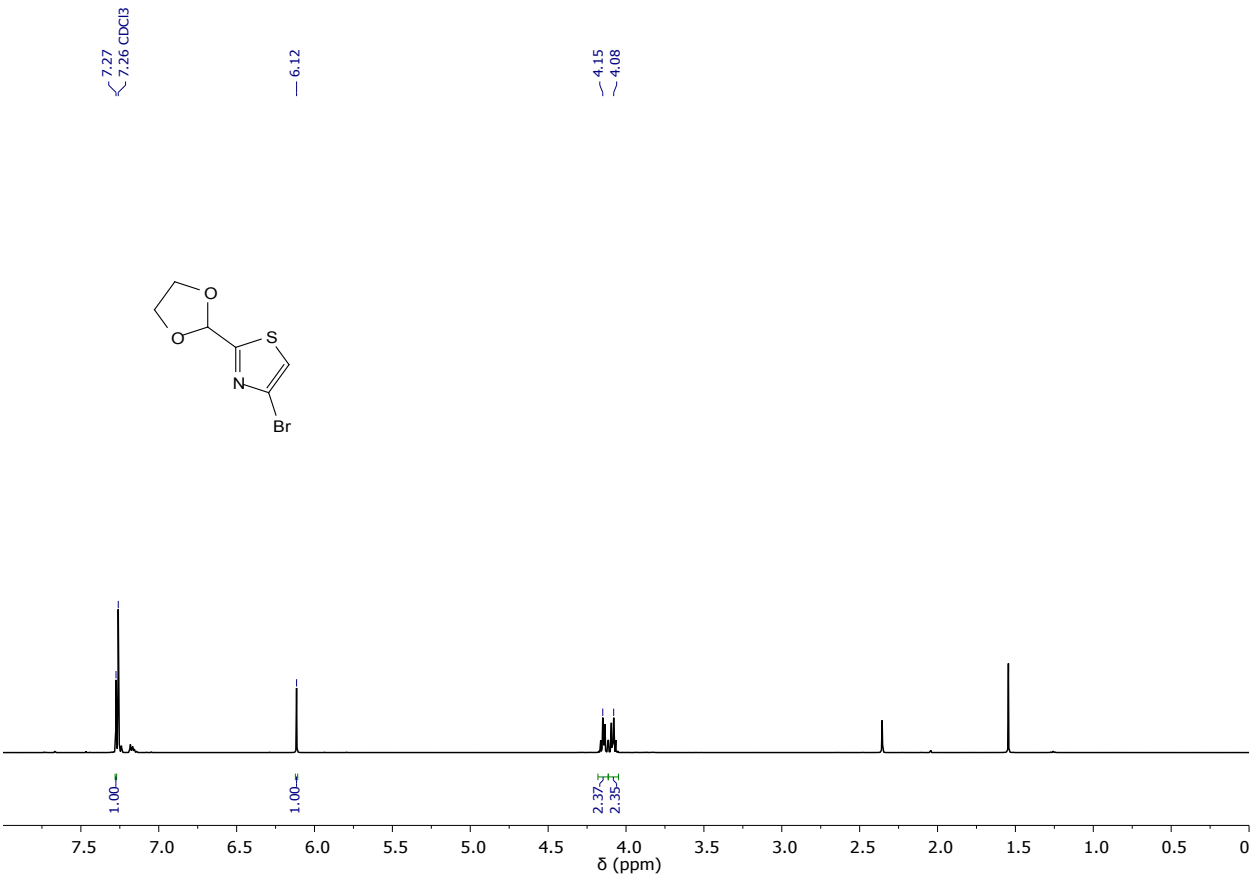

Figure S1. ^{1}H-NMR spectrum of compound **1**.

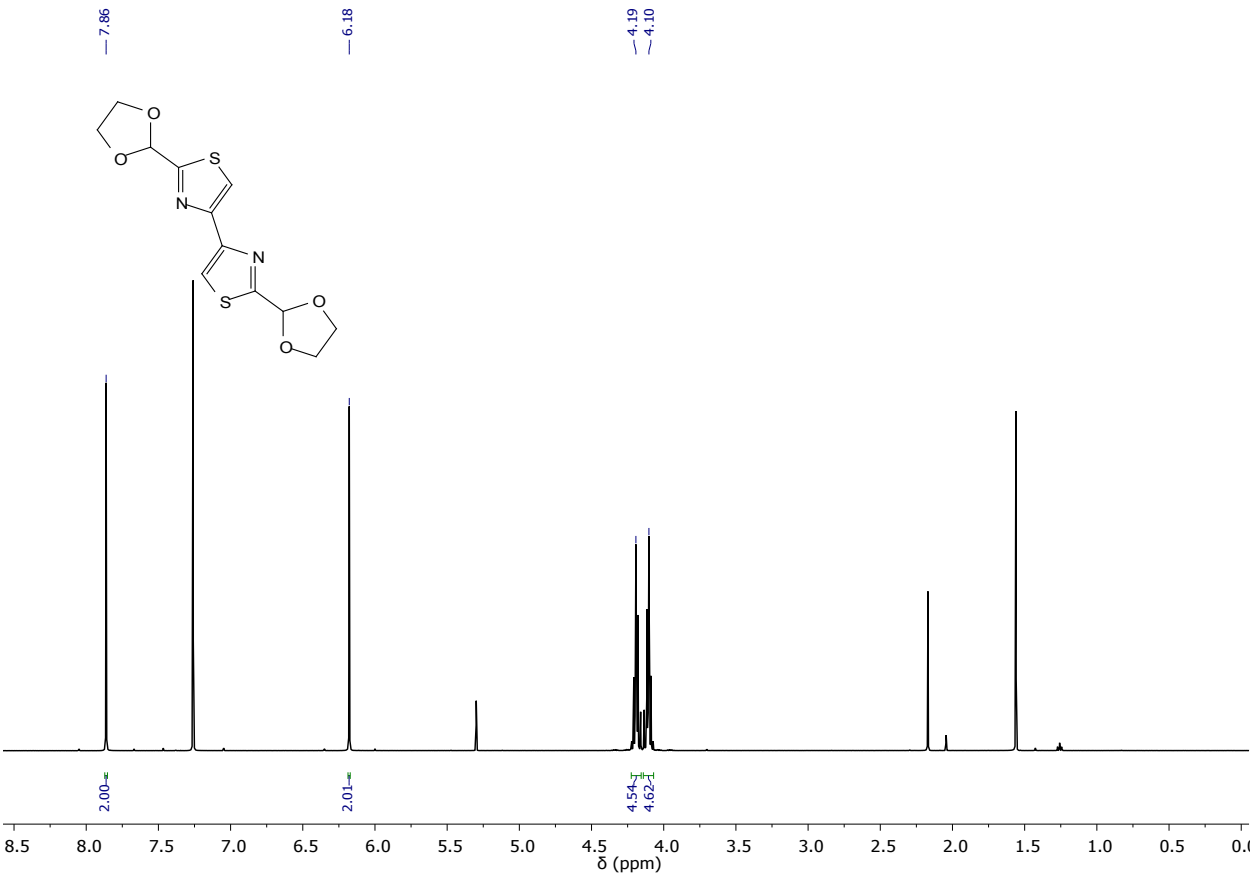

Figure S2. [1]H-NMR spectrum of compound **2**.

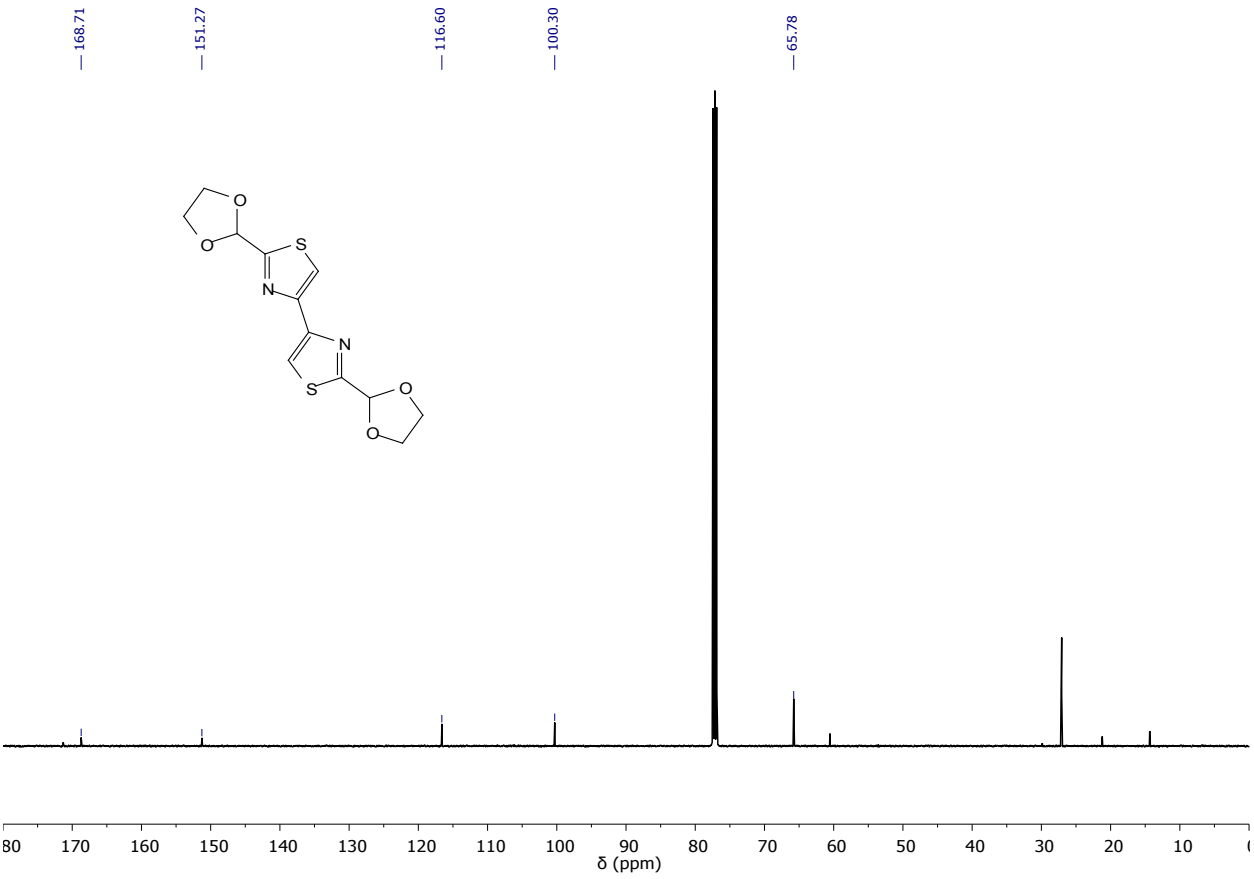

Figure S3. ^{13}C NMR spectrum of compound **2**.

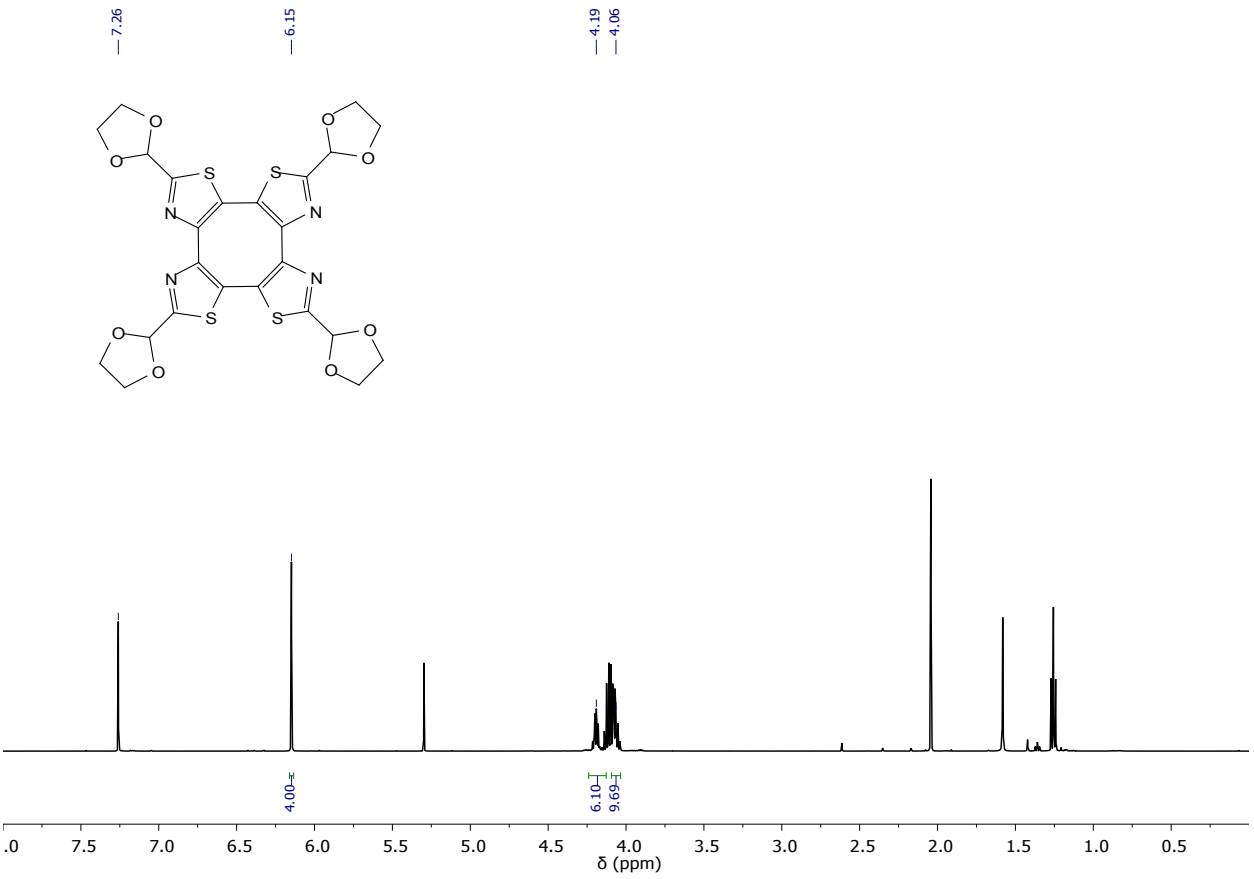

Figure S4. ^{1}H NMR spectrum of compound **3**.

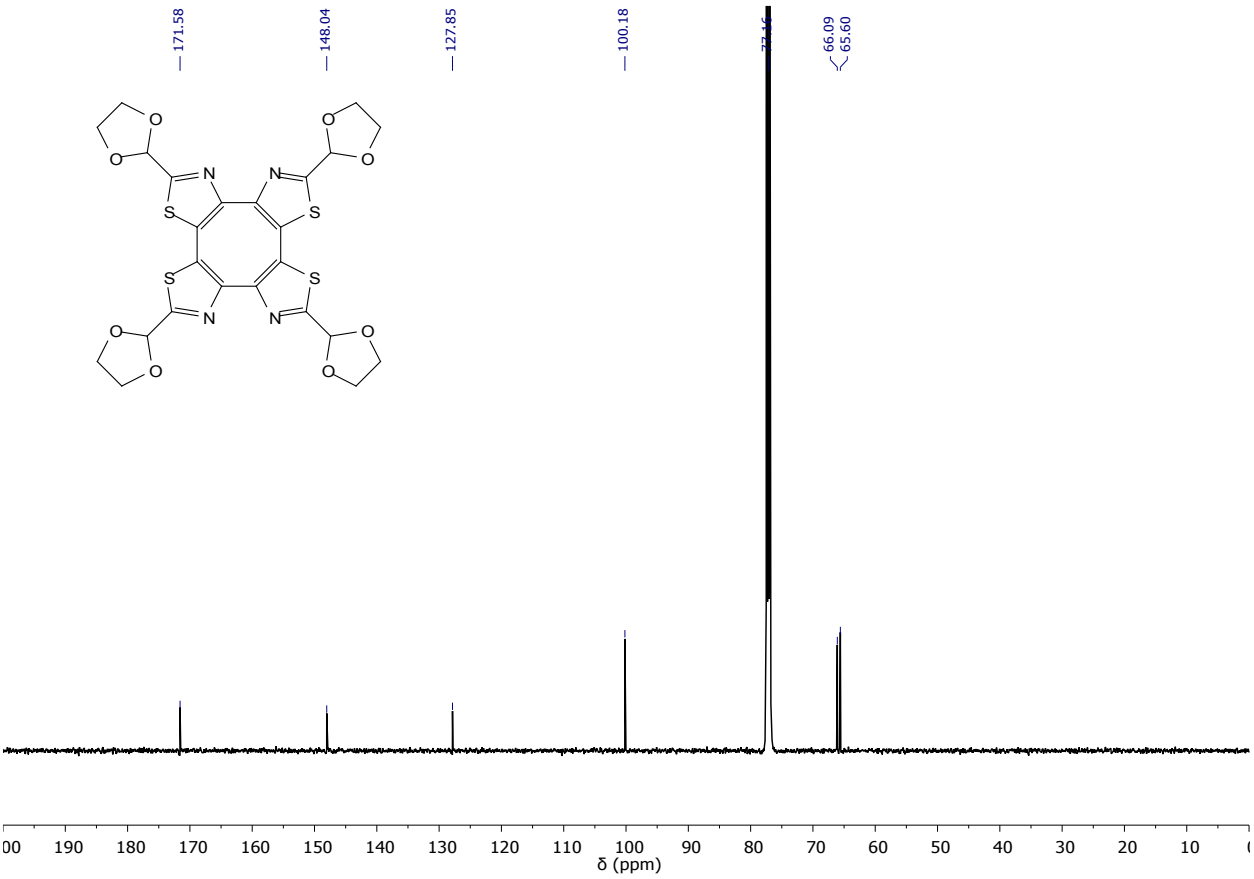

Figure S5. ^{13}C NMR spectrum of compound **3**.

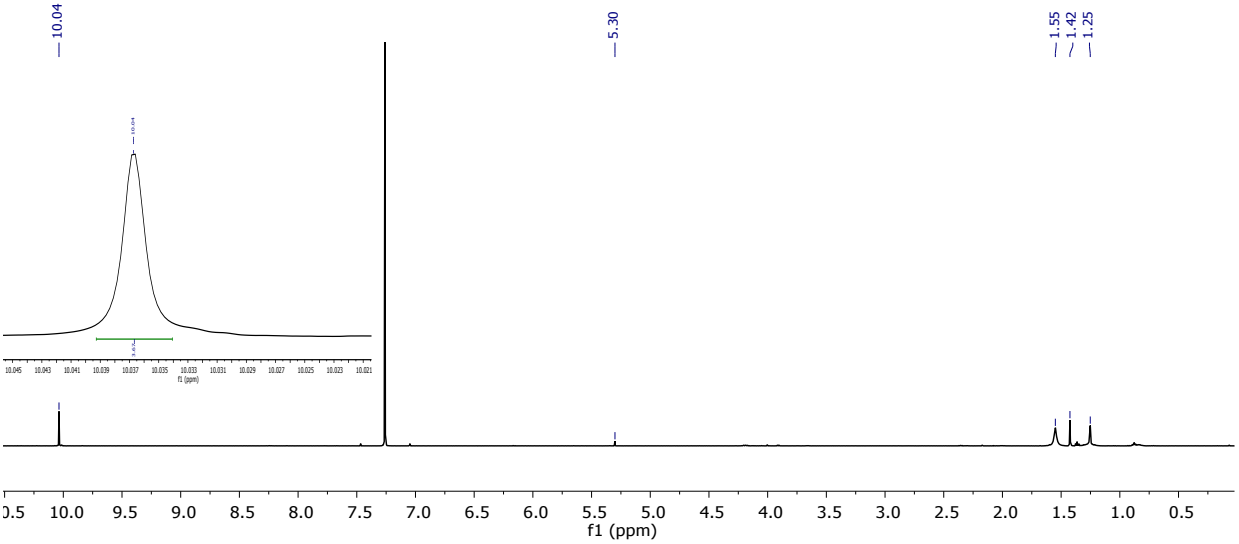

Figure S6. ^{1}H NMR spectrum of compound **4** (COTz(CHO)$_4$). Inse: Magnification of the range 10.05 to 10.02 ppm.

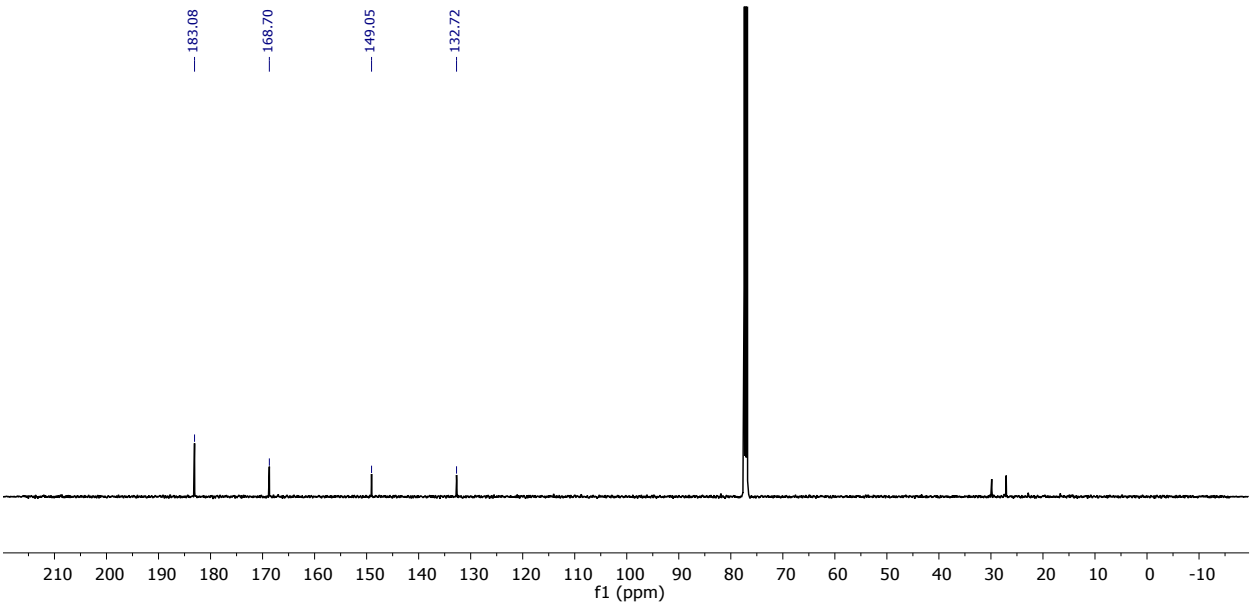

Figure S7. ^{13}C NMR spectrum of COTz(CHO)$_4$ (**4**).

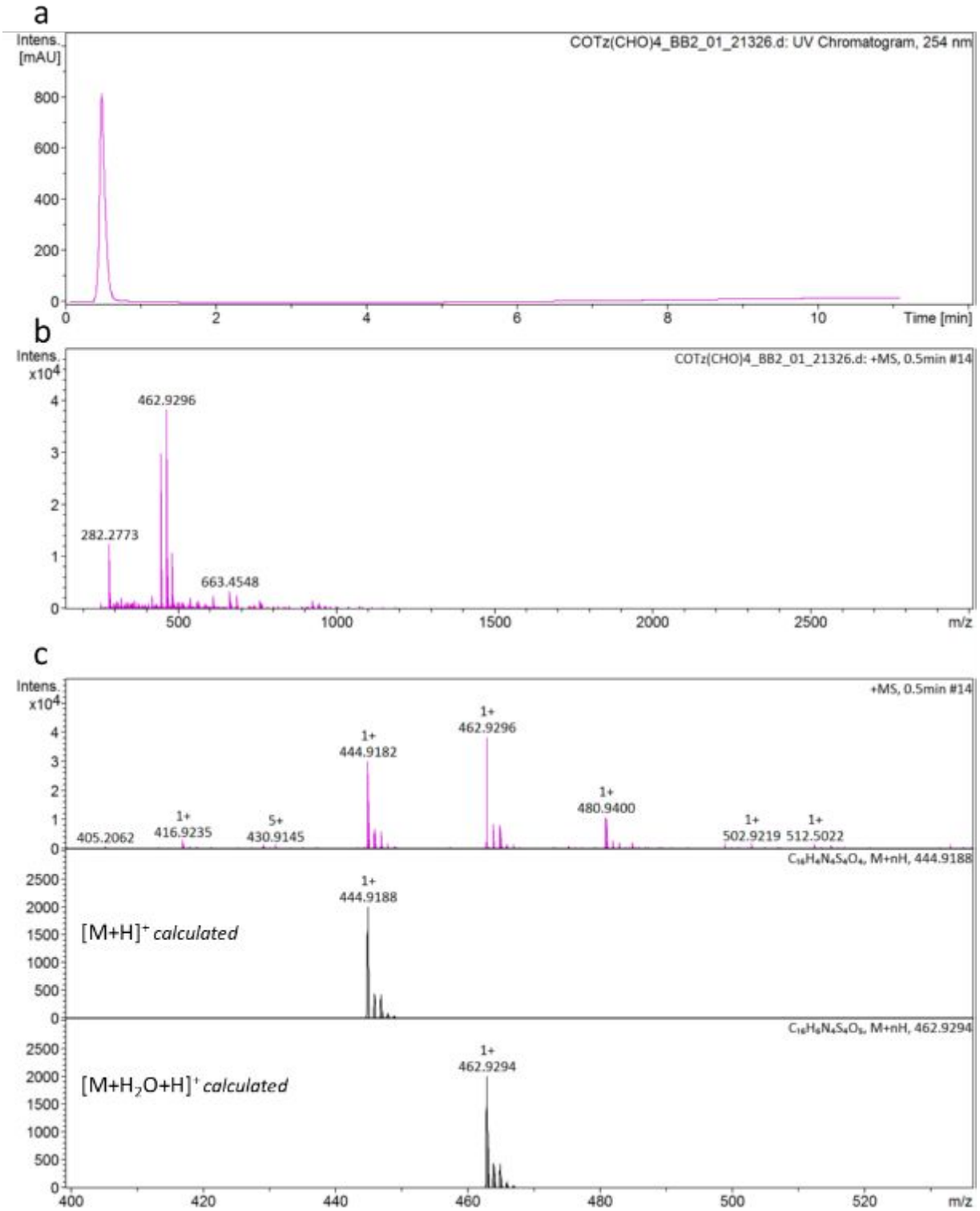

Figure S8. HRMS of COTz(CHO)$_4$ (**4**). (a) Chromatogram of COTz(CHO)$_4$ building block, linear gradient from 70% acetonitrile (30% water) to 100% acetonitrile, stationary phase InfinityLab Poroshell 120 SB-C18, 2.1 mm, 1.9 µm column. (b) Full MS spectrum of COTz(CHO)$_4$. (c) Magnification of MS from m/z 400 to 500. The calculated values for $[M+H]^+$ and $[M+H_2O+H]^+$, respectively, are given in black.

Table S1. Crystallographic data for the $COTz(CHO)_4$ bulding block (compound **4**).

Identification code CCDC	2513710
Empirical formula	$C_{16}H_4N_4O_4S_4$
Formula weight	444.47
Temperature/K	173.00(10)
Crystal system	monoclinic
Space group	C2/c
a/Å	27.4820(7)
b/Å	8.57151(7)
c/Å	19.2314(5)
α/°	90
β/°	132.842(4)
γ/°	90
Volume/Å^3	3321.7(2)
Z	8
ρ_{calc}g/cm^3	1.778
μ/mm^{-1}	5.595
F(000)	1792.0
Crystal size/mm^3	0.25 × 0.1 × 0.02
Radiation	Cu Kα (λ = 1.54184)
2Θ range for data collection/°	8.776 to 150.124
Index ranges	$-33 \leq h \leq 34$, $-10 \leq k \leq 8$, $-23 \leq l \leq 23$
Reflections collected	28815
Independent reflections	3369 [R_{int} = 0.0406, R_{sigma} = 0.0202]
Data/restraints/parameters	3369/0/258
Goodness-of-fit on F^2	1.076
Final R indexes [I>=2σ (I)]	R_1 = 0.0344, wR_2 = 0.0956
Final R indexes [all data]	R_1 = 0.0364, wR_2 = 0.0974
Largest diff. peak/hole / e Å^{-3}	0.55/-0.27

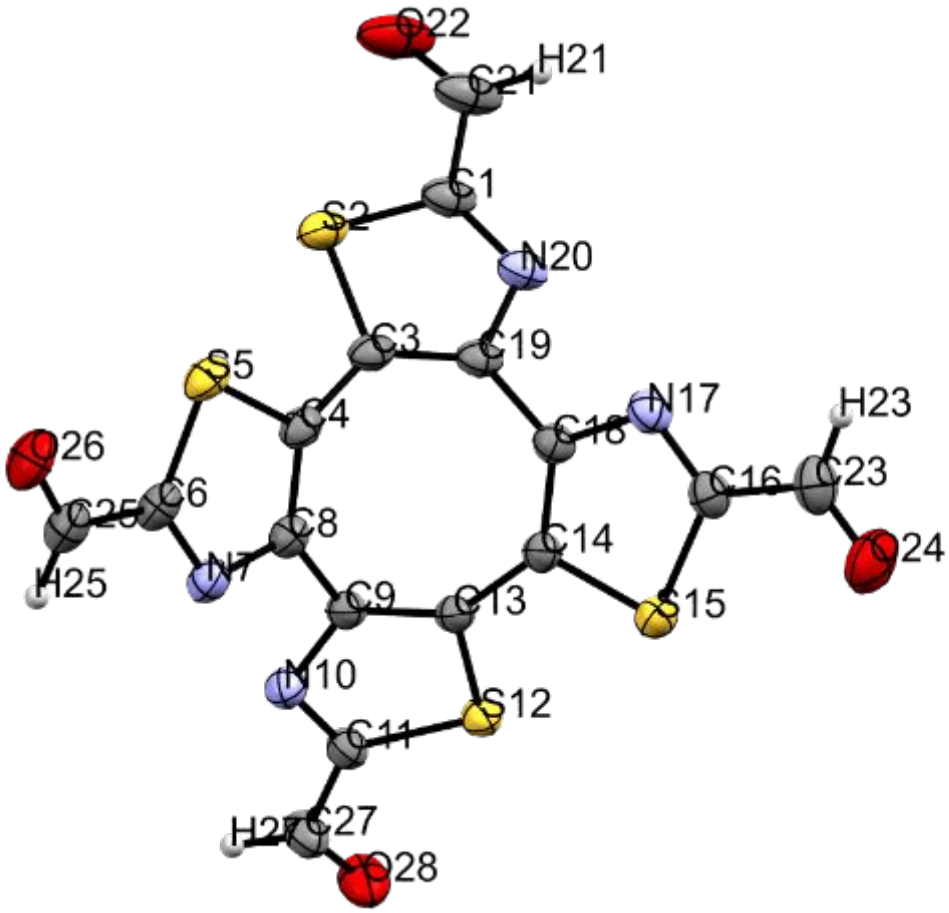

Figure S9. Crystal structure of the COTz(CHO)$_4$ building block (**4**). Ellipsoids indicating anisotropic displacement are drawn at 50% probability level.

Table S2. . Fractional Atomic Coordinates ($\times 10^4$) and Equivalent Isotropic Displacement Parameters ($Å^2 \times 10^3$) for compound CCDC 2513710 (**4**). U_{eq} is defined as 1/3 of the trace of the orthogonalised U_{IJ} tensor.

Atom	*x*	*y*	*z*	*U(eq)*
S12	8347.4(2)	4332.6(6)	9246.3(3)	28.69(13)
S5	5440.1(2)	1532.6(6)	5722.1(4)	34.41(15)
S15	8569.2(2)	2145.4(6)	8032.2(3)	31.05(14)
S2	5553.7(3)	4668.5(6)	4840.6(4)	37.18(15)
O26	4816.5(8)	-826(2)	6097.6(13)	50.1(4)
O28	8597.5(9)	5626(2)	10916.4(12)	50.9(5)
N10	7272.3(8)	3591.0(19)	8853.3(12)	29.6(4)
N20	6660.0(9)	4939(2)	5262.8(12)	34.1(4)
N17	7696.3(9)	2679(2)	6237.3(12)	32.3(4)
N7	6303.3(8)	1367(2)	7540.5(13)	32.3(4)
O24	9227.6(9)	861(2)	7354.6(15)	59.6(5)
O22	5230.3(12)	7112(2)	3443.6(13)	68.4(6)
C14	7826.6(9)	3002(2)	7554.7(13)	26.6(4)
C13	7720.1(9)	3442(2)	8173.2(13)	26.0(4)
C4	6156.7(9)	2618(2)	6335.5(13)	29.1(4)
C19	6772.0(10)	3936(2)	5917.4(13)	29.0(4)
C18	7429.9(10)	3200(2)	6594.0(14)	27.7(4)
C9	7185.1(9)	3153(2)	8083.6(13)	26.7(4)
C11	7855.5(10)	4226(2)	9502.1(14)	30.2(4)
C8	6554.0(9)	2376(2)	7294.6(14)	28.6(4)
C3	6230.8(10)	3655(2)	5810.2(13)	29.2(4)
C6	5721.6(10)	857(2)	6783.8(15)	33.4(4)
C25	5313.6(11)	-254(3)	6802.9(18)	39.7(5)
C16	8288.1(11)	2108(2)	6915.1(15)	32.7(4)
C1	6041.9(12)	5404(3)	4660.2(15)	36.6(5)
C27	8083.9(12)	4919(3)	10384.9(16)	39.4(5)
C23	8685.2(13)	1393(3)	6733.5(19)	43.2(5)
C21	5767.5(15)	6533(3)	3887.5(16)	48.4(6)

Table S3. Components U_{ij} of the Anisotropic Displacement Parameters (Å^2×10^3) for CCDC 2513710 (**4**).

Atom	U_{11}	U_{22}	U_{33}	U_{23}	U_{13}	U_{12}
S12	25.3(2)	34.4(3)	23.5(2)	-3.00(17)	15.5(2)	-5.28(18)
S5	23.6(2)	35.6(3)	30.9(3)	-5.31(19)	13.3(2)	-3.03(18)
S15	27.6(2)	33.2(3)	31.3(3)	3.10(19)	19.7(2)	2.85(18)
S2	32.4(3)	41.4(3)	25.5(3)	1.9(2)	14.9(2)	9.9(2)
O26	31.7(8)	50.1(10)	58.3(11)	-8.3(8)	26.5(8)	-10.6(7)
O28	44.4(9)	71.3(12)	36.8(9)	-21.4(8)	27.6(8)	-21.3(9)
N10	26.7(8)	33.5(9)	27.2(8)	-2.6(6)	17.8(7)	-1.5(7)
N20	42.6(10)	33.2(9)	27.6(8)	2.3(7)	24.4(8)	6.0(8)
N17	36.6(9)	33.2(9)	31.1(9)	-1.7(7)	24.6(8)	1.2(7)
N7	24.7(8)	33.4(9)	33.8(9)	1.8(7)	17.9(7)	-1.0(7)
O24	47.0(10)	64.0(12)	68.5(13)	-1.8(10)	39.6(10)	14.4(9)
O22	88.8(15)	66.0(13)	37.9(9)	17.3(9)	38.0(10)	45.5(12)
C14	25.6(9)	27.4(9)	26.1(9)	0.2(7)	17.3(8)	-1.3(7)
C13	24.4(9)	27.3(9)	22.5(9)	1.2(7)	14.5(8)	-0.9(7)
C4	24.2(9)	29.9(9)	26.9(9)	-5.2(7)	14.9(8)	-0.6(7)
C19	33.3(10)	29.3(9)	22.2(9)	-1.6(7)	18.0(8)	2.0(8)
C18	29.7(9)	27.0(9)	26.8(9)	-0.8(7)	19.3(8)	-0.3(7)
C9	25.6(9)	28.8(9)	23.2(9)	0.7(7)	15.6(8)	-0.5(7)
C11	31.2(10)	34.1(10)	27.9(10)	-2.1(8)	21.1(9)	-2.3(8)
C8	24.2(9)	29.6(9)	27.8(9)	-1.2(8)	16.1(8)	-0.5(7)
C3	28.3(9)	30.3(10)	21.6(9)	-2.6(7)	14.0(8)	3.9(8)
C6	23.5(9)	31.6(10)	36.7(11)	-0.2(8)	17.2(9)	1.3(8)
C25	28.1(10)	37.8(12)	46.4(13)	3.0(10)	22.7(10)	0.7(9)
C16	36.4(10)	31.3(10)	36.6(11)	-1.5(8)	27.3(9)	0.8(8)
C1	46.4(12)	34.9(11)	26.1(10)	0.7(8)	23.8(10)	8.4(9)
C27	40.9(12)	50.7(13)	32.5(11)	-9.4(10)	27.3(10)	-10.1(10)
C23	47.6(13)	41.1(12)	55.3(14)	-4.0(10)	40.6(13)	2.8(10)
C21	72.3(17)	38.1(12)	32.5(12)	6.3(9)	34.8(13)	19.2(12)

Table S4. Bond lengths for CCDC 2513710 (**4**).

Atom	Atom	Length/Å		Atom	Atom	Length/Å
S12	C13	1.7249(19)		N7	C8	1.375(3)
S12	C11	1.727(2)		N7	C6	1.304(3)
S5	C4	1.725(2)		O24	C23	1.198(3)
S5	C6	1.719(2)		O22	C21	1.200(3)
S15	C14	1.7316(19)		C14	C13	1.455(3)
S15	C16	1.719(2)		C14	C18	1.375(3)
S2	C3	1.725(2)		C13	C9	1.381(3)
S2	C1	1.718(2)		C4	C8	1.378(3)
O26	C25	1.194(3)		C4	C3	1.460(3)
O28	C27	1.201(3)		C19	C18	1.470(3)
N10	C9	1.381(2)		C19	C3	1.377(3)
N10	C11	1.305(3)		C9	C8	1.475(3)
N20	C19	1.376(3)		C11	C27	1.477(3)
N20	C1	1.308(3)		C6	C25	1.491(3)
N17	C18	1.375(3)		C16	C23	1.485(3)
N17	C16	1.304(3)		C1	C21	1.480(3)

Table S5. Bond angles for CCDC 2513710 (**4**).

Atom	Atom	Atom	Angle/°		Atom	Atom	Atom	Angle/°
C13	S12	C11	88.75(9)		N10	C9	C8	116.81(17)
C6	S5	C4	89.24(10)		C13	C9	C8	128.07(18)
C16	S15	C14	88.80(10)		N10	C11	S12	116.12(15)
C1	S2	C3	89.23(10)		N10	C11	C27	123.56(19)
C11	N10	C9	110.09(16)		C27	C11	S12	120.21(16)
C1	N20	C19	110.41(19)		N7	C8	C4	115.38(17)
C16	N17	C18	110.40(17)		N7	C8	C9	116.38(17)
C6	N7	C8	110.35(18)		C4	C8	C9	128.06(18)
C13	C14	S15	119.74(14)		C4	C3	S2	119.94(15)
C18	C14	S15	109.68(14)		C19	C3	S2	109.58(15)
C18	C14	C13	130.53(18)		C19	C3	C4	130.36(18)
C14	C13	S12	120.01(14)		N7	C6	S5	115.65(16)
C9	C13	S12	109.98(14)		N7	C6	C25	123.9(2)
C9	C13	C14	129.81(17)		C25	C6	S5	120.40(16)
C8	C4	S5	109.36(15)		O26	C25	C6	122.2(2)
C8	C4	C3	131.39(18)		N17	C16	S15	115.93(15)
C3	C4	S5	119.11(14)		N17	C16	C23	122.4(2)
N20	C19	C18	116.96(18)		C23	C16	S15	121.59(17)
N20	C19	C3	115.21(18)		N20	C1	S2	115.56(16)
C3	C19	C18	127.64(18)		N20	C1	C21	123.9(2)
N17	C18	C14	115.19(18)		C21	C1	S2	120.55(19)
N17	C18	C19	116.72(17)		O28	C27	C11	121.1(2)
C14	C18	C19	128.06(18)		O24	C23	C16	122.5(2)
N10	C9	C13	115.05(17)		O22	C21	C1	121.7(3)

Table S6. Hydrogen atom coordinates (Å×10^4) and Isotropic Displacement Parameters (Å^2×10^3) for CCDC 2513710 (**4**).

Atom	*x*	*y*	*z*	*U(eq)*
H25	5453.75	-516.85	7395.99	48
H27	7784(14)	4800(30)	10461(19)	47
H23	8502.18	1357.42	6100.69	52
H21	6022.95	6806.55	3738.87	58

3. COF synthesis:

The preparation of the COF based on the pseudotetrahedral building block $COTz(CHO)_4$ was conducted in a globe box under argon atmosphere. Solvents and acetic acid were obtained in high purity grade from commercial suppliers and were, unless shipped under inert gas, degassed and flushed with argon prior to use.

$COTz(CHO)_4$ (**4**) (4.44 mg, 10 µmol, 1.0 eq), aniline (18.3 µL, 200 µmol, 20 eq), a solvent mixture of benzyl alcohol and dioxane (1:1, v/v; 125 µL) and 6 M acetic acid (25 µL) were added into a 5 mL culture tube under argon atmosphere. Subsequently, *p*-phenylenediamine (2.16 mg, 20 µmol, 2.0 eq.) and additional 125 µL of the solvent mixture were added. The reaction tube was sealed and heated at 120 °C for 3 d. After cooling to room temperature, the precipitate was filtrated and washed with dry tetrahydrofuran. Extraction with supercritical CO_2 yielded the COF COTz-1P as a dark-red powder. (3.65 mg, 62% yield)

4. Scanning electron microscopy (SEM):

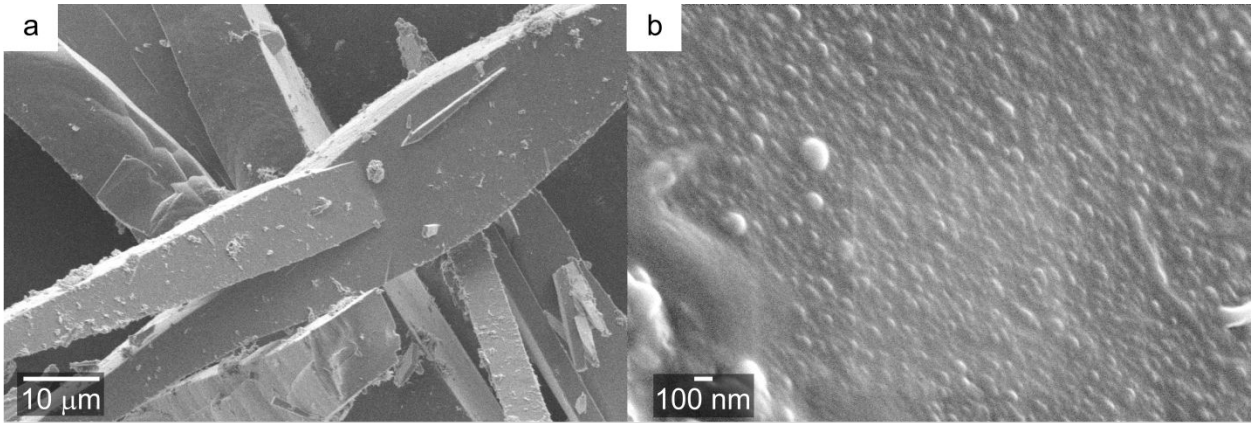

Figure S10. (a) Low-magnification SEM image showing the overall morphology of needle-like molecular crystals of the $COTz(CHO)_4$ building block. (b) High-magnification SEM image focusing on the surface of a single crystal.

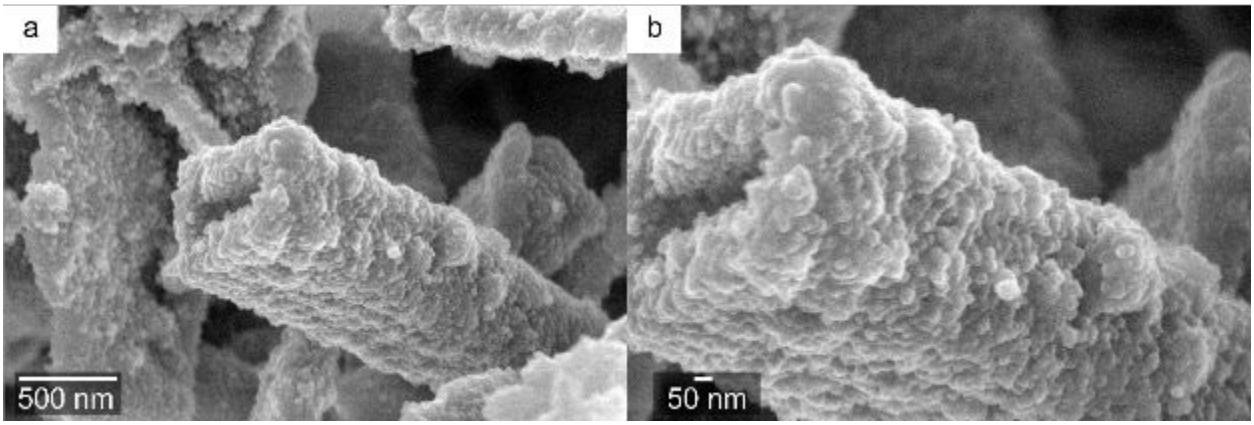

Figure S11. (a) SEM image showing the morphology of the COTz-1P COF. The material exhibits a well-defined hollow, rectangular tube-microrod morphology, with width of approximately 500 nm. (b) SEM image of a single COF architecture at higher magnification, revealing a highly granular and hierarchical porous structure. The structure appears to be composed of small, densely packed nanoparticles or crystalline domains.

5. Transmission Electron Microscopy (TEM):

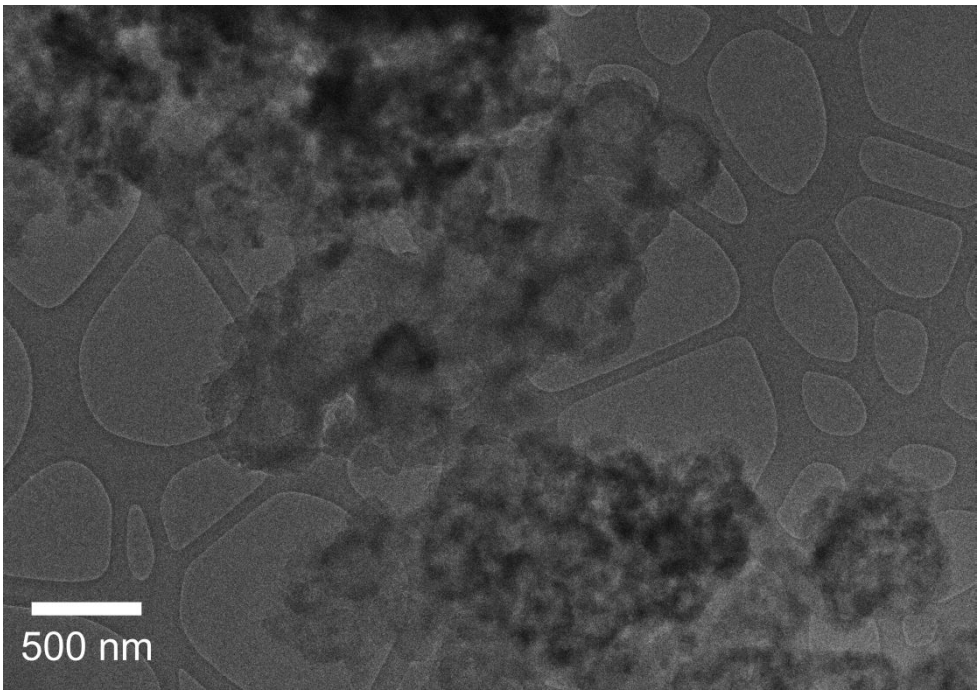

Figure S12. TEM overview image of the COTz-1P COF. The image reveals large, electron-dense agglomerates with internal contrast variations. The lighter regions within the darker features suggest a hollow or porous interior, consistent with the tubular architecture observed in Figure S11.

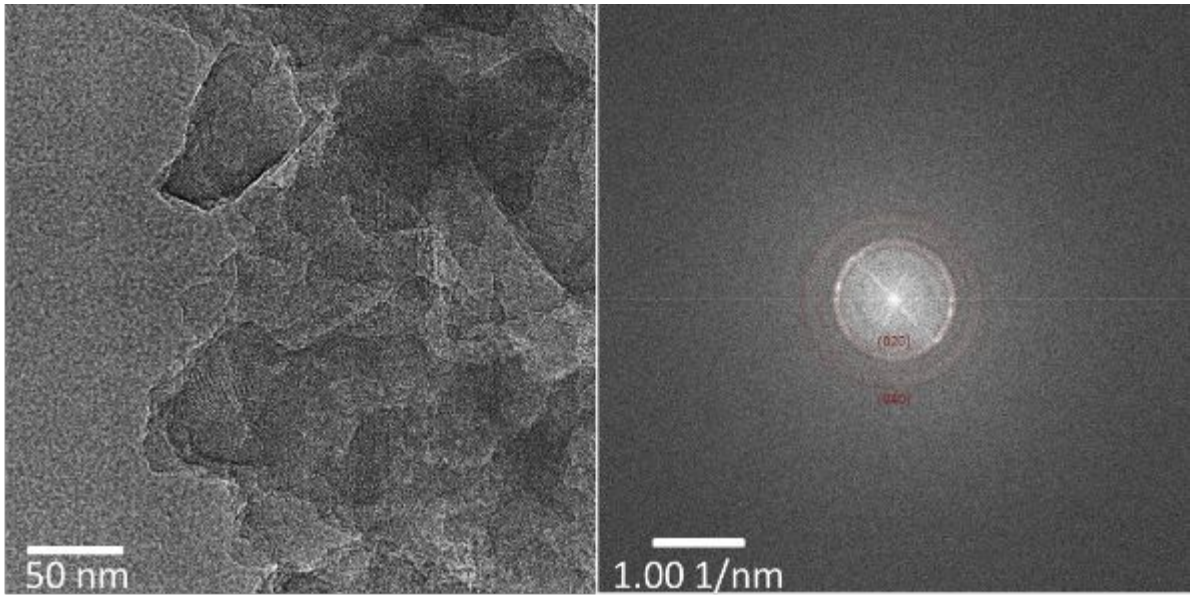

Figure S13. a) Transmission electron microscopy (TEM) image of the COTz-1P COF, illustrating the local framework morphology and internal structure. b) Corresponding Fast Fourier Transform (FFT) pattern obtained from (a), showing the planes (020) and (040), respectively.

6. Optical Characterization:

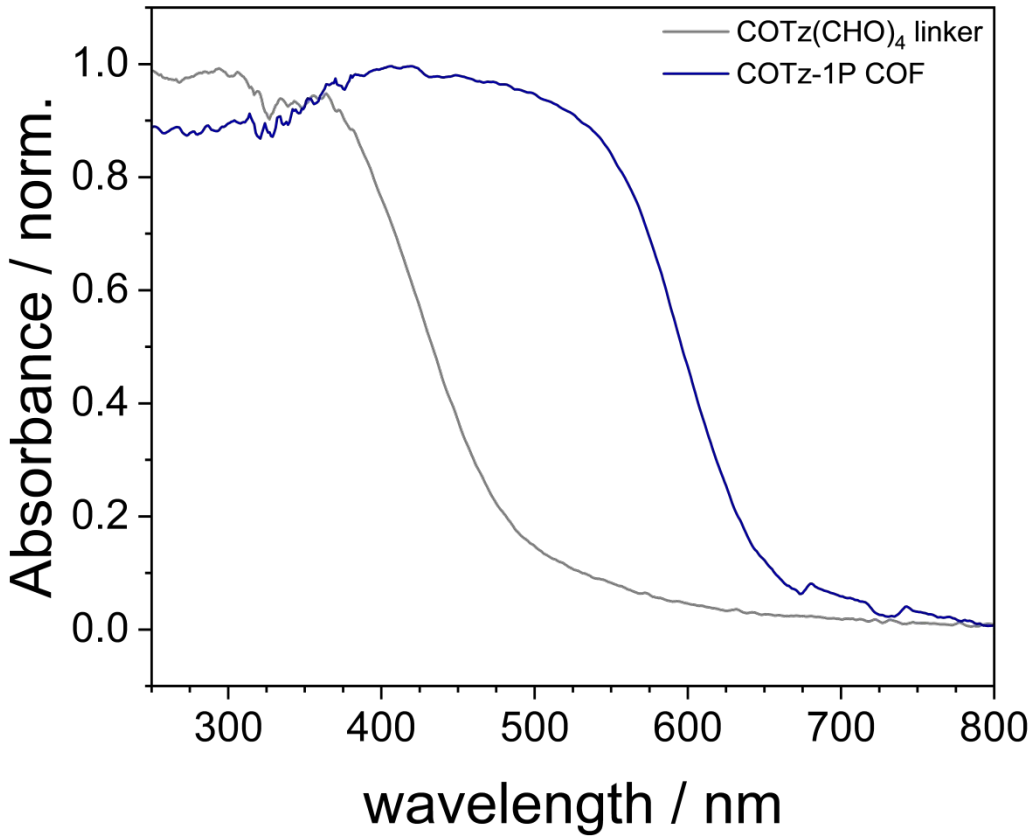

Figure S14. Normalized UV–Vis absorption spectra of the $COTz(CHO)_4$ linker (gray) and the corresponding COTz-1P COF (blue), both as powder. Formation of the COF results in a pronounced red shift of the optical absorption, indicating extended π-conjugation and enhanced visible light absorption upon COF formation.

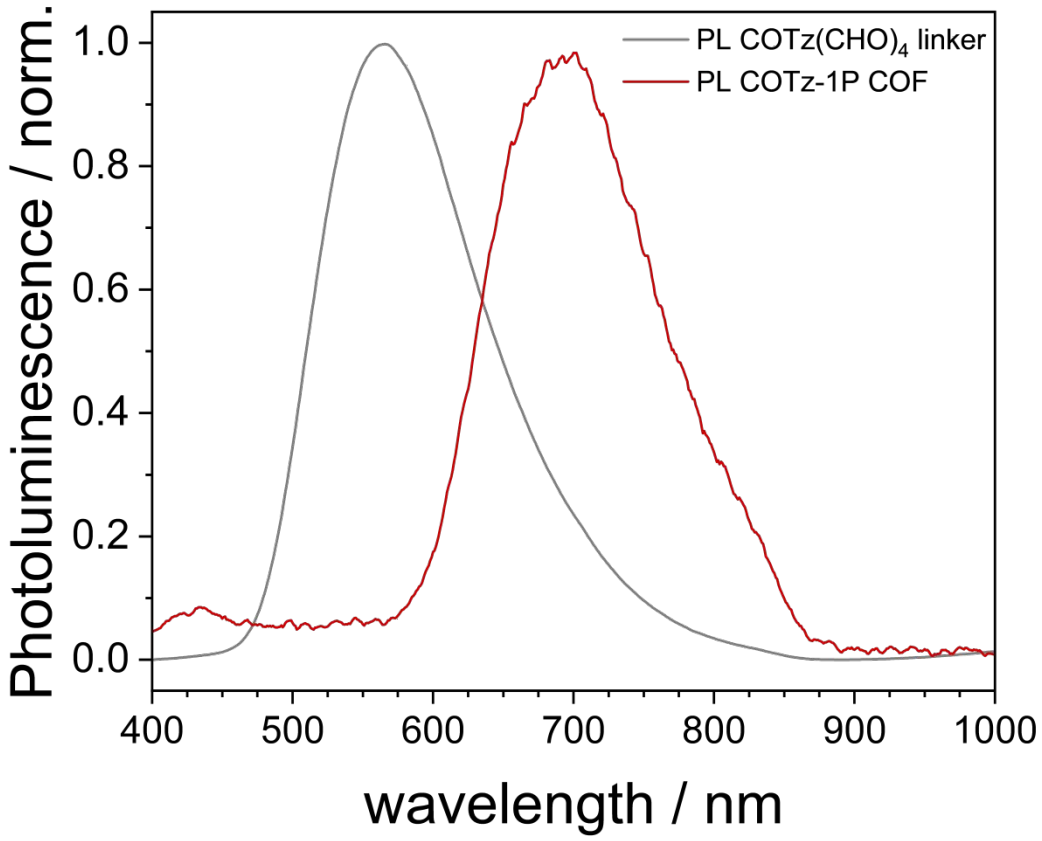

Figure S15. Normalized photoluminescence (PL) spectra of the $COTz(CHO)_4$ linker (gray) and the corresponding COTz-1P COF (red), both as powder. The spectra show a pronounced red shift upon framework formation, indicative of an increased conjugation in the COF.

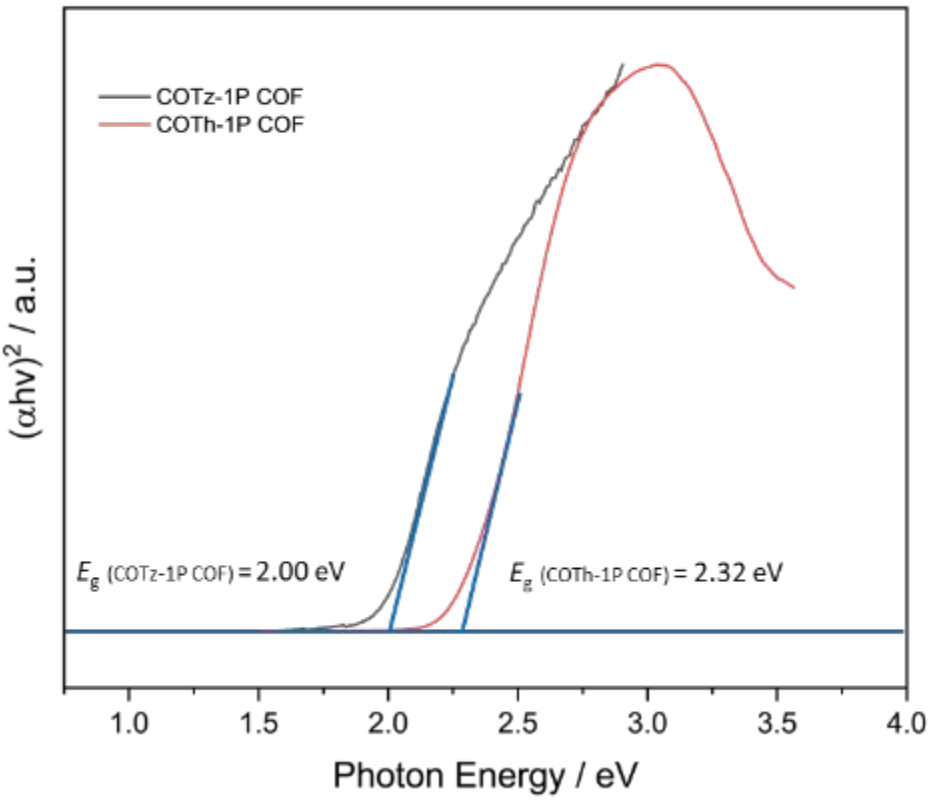

Figure S16. Comparison of the optical band gap (obtained via Tauc plot) for the previously reported, related thiophene-based 3D conjugated COF (red line, COTh-1P COF) [5] and the thiazole-based COF presented in this work (black line, COTz-1P COF). The optical band gap of the new COF is 0.32 eV lower compared to the thiophene-based one. For both COFs, a direct band gap was assumed.

7. Structural Analysis:

Table S7. Unit cell parameters and atomic coordinates for the COTz-1P COF.

Unit cell parameters (space group $I4_1$) and atomic coordinates for COTz-1P COF				
		***a* = *b* = 30.104582 Å, *c* = 4.389641 Å**		
		$\alpha = \beta = \gamma = 90.000°$		
		Volume = 3978.269 Å^3		
Atoms	Element	*a/x*	*b/y*	*c/z*
C1	C	0.56206	0.52273	0.55023
S2	S	0.61123	0.53502	0.6941
C3	C	0.61844	0.48152	0.76049
C4	N	0.58726	0.45536	0.66425
C5	C	0.55481	0.47809	0.54701
N6	N	0.68856	0.49283	0.03611
C7	C	0.65724	0.46556	-0.00781
C8	C	0.75852	0.52106	0.1554
C9	C	0.73895	0.45083	0.33666
C10	C	0.72889	0.48713	0.17502
C11	C	0.45611	1.00357	0.62407
C12	N	0.41886	0.99291	0.49569
C13	C	0.39787	0.01037	0.40684
S14	S	0.42028	0.05832	0.49597
C15	C	0.46289	0.03032	0.63583
N16	N	0.33765	0.99264	0.17317
C17	C	0.35761	0.00999	0.24842
C18	C	0.2695	0.95846	0.93577
C19	C	0.28864	0.01081	0.75219
C20	C	0.2987	0.99332	0.01106
H22	H	0.65907	0.43207	0.05606
H23	H	0.75075	0.54885	0.02937
H24	H	0.71614	0.42445	0.35825
H26	H	0.34444	0.04162	0.20202
H27	H	0.27699	0.93109	1.0656
H28	H	0.31096	0.03747	0.72548

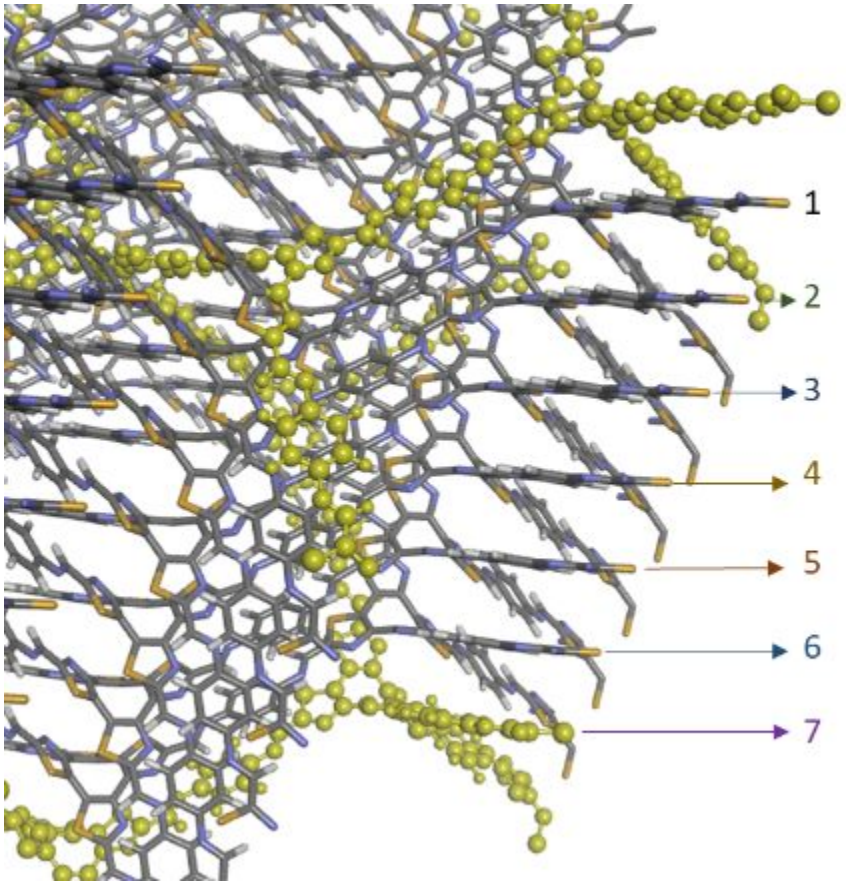

Figure S17. Visualization of the interpenetration level of the COTz-1P COF. Tilted side view onto the structure simulation, with a single fragment highlighted (yellow) showing the 7-fold interpenetration of the 3D COF.

8. References:

[1] Rigaku-Oxford-Diffraction, CrysAlisPro Software system, version 1.171.43.130a, **2024**, Rigaku Corporation, Wroclaw, Poland.

[2] Rigaku-Oxford-Diffraction, AutoChem 6.0 software system in conjunction with Olex2 1.5-ac6, **2024**, Rigaku Corporation, Wroclaw, Poland.

[3] Sheldrick, G. M., A Short History of SHELX. *Acta Crystallogr. Sect. A: Found. Crystallogr*., **2008**, 64, 112-122.

[4] Dolomanov, O. V.; Bourhis, L. J.; Gildea, R. J.; Howard, J. A.; Puschmann, H., OLEX2: a complete structure solution, refinement and analysis program. *J. Appl. Crystallogr.*, **2009**, 42, 339-341.

[5] Munoz-Alonso, I.; Bessinger, D.; Reuter, S.; Righetto, M.; Fuchs, L.; Döblinger, M.; Medina, D. D.; Ortmann, F.; Herz, L. M.; Bein, T., Highly Crystalline and Oriented Thin Films of Fully Conjugated 3D-Covalent Organic Frameworks. *Angewandte Chemie International Edition* **2025,** *64* (34), e202505799.